UC Davis

UC Davis Previously Published Works

Title

Probing the initial stages of iron surface corrosion: Effect of O2 and H2O on surface carbonation

Permalink

Authors

de Alwis, Chathura
Trought, Mikhail
Crumlin, Ethan J
et al.

Publication Date

DOI

Copyright Information

Peer reviewed

Probing the Initial Stages of Iron Surface Corrosion:

## Effect of O_2 and H_2O on Surface Carbonation

Chathura de Alwis[1], Mikhail Trought[1], Ethan J. Crumlin[2], Slavomir Nemsak[2,3], Kathryn A. Perrine[1*]

[1]Department of Chemistry, Michigan Technological University, Houghton, MI 49931;

[2]Advanced Light Source, Lawrence Berkeley National Laboratory, CA 94720, United States of America

[3]Department of Department of Physics and Astronomy, University of California, Davis, CA 95616

*Corresponding author, kaperrin@mtu.edu
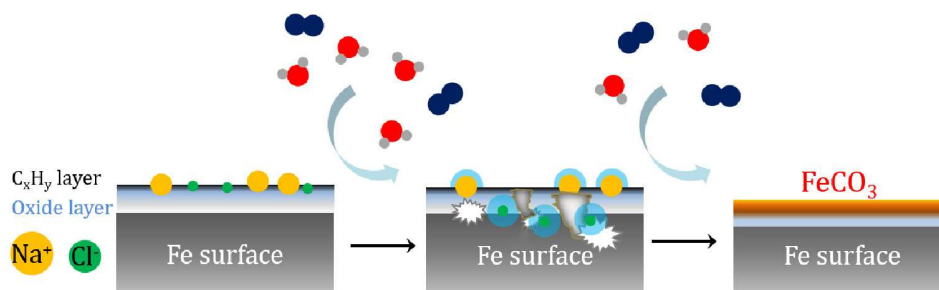
Abstract

Iron plays a vital role in natural processes such as water, mineral, iron, and nutrient cycles. Iron undergoes reduction-oxidation and catalytic reactions to produce various corrosion films depending on its chemical environment. Near ambient pressure X-ray photoelectron spectroscopy, polarized modulated infrared reflection absorption spectroscopy, and Auger electron spectroscopy were used to study the key reactants, from $O_2(g)$, H_2O vapor, and Na^+ and Cl^- on the initial stages of iron surface corrosion. With increasing the ratio of O_2 and H_2O, surface hydrocarbons were shown to oxidize into carbonates, while the Cl^- were found to migrate into the interface. The effect of each individual reactant was measured separately and water was shown to have a first order rate dependence on the carbonate growth at low pressures, with little dependence for O_2. Near ambient pressures, both H_2O and O_2 were found in increase the carbonate growth, which was estimated using the Langmuir isotherm model, yielding Gibbs energies between -9.8 to -8.5 kJ/mol. A mechanism is suggested to explain the oxidation is catalyzed by NaCl on iron surfaces and the adventitious hydrocarbons served as the source for surface carbonation. These findings have implications for understanding other surface catalytic and redox interface chemistry in complex environments.

[1] Present address: Ford Motor Company; Manufacturing Research Dept., Ford Research and Advanced Engineering; Research and Innovation Center; 2101 Village Road, Room 1323, MD 3135 Dearborn, MI 48121 USA

1.0 Introduction

The deterioration of metals due to the interaction with their environment is known as corrosion. Metallic iron (Fe) is the primary element in the composition of steel and has been used for industrial and technological purposes since the prehistoric era, due to its high natural abundance, good processability, high strength, and easy extractability. Although Fe delivers many advantages in terms of industrial and technological applications, its main drawback is the corrosion from environmental factors.[1] The corrosion of Fe causes severe deteriorations in automobiles, ship hulls, bridges, machine tools[2], structural components of buildings, and water pipelines causing safety concerns.[3] [4] Aside from corrosion, iron performs a vital role in nature through mineral cycling of Fe in the natural environment in soils, atmospheric dust[5] [6], and geological mineralization.[7] In these natural conditions, iron undergoes reduction and oxidation (redox) reactions[8] affecting pollutant degradation[9], delivering nutrients to plants, and mineral film growth.[10]

Corrosion challenges involve multiple length scales, from the micrometer level down to the nanoscale.[11] Electrochemical methods have been used to measure electron transfer processes at liquid/solid interfaces, but are unable to directly measure the state of the surface during the redox reactions. Previous studies use methods to measure the rate of corrosion[12] [13] [14] and composition of corrosion products.[15] [16] [17] However in liquid environments, where environmental conditions (from aquatic marine water, salty air, high temperature steel corrosion, oil drilling pipeline corrosion) are complex due to simultaneous presence of the ions, dissolved organic matter, microbes, and gases that react with the surface that is undergoing dynamic redox reactions.[18] To study the initial stages of iron corrosion, the physical and chemical changes can be measured using surface analysis at the nano and molecular scale to provide a detailed description at the fundamental level. [11, 19, 20] [21]

In the chemical process of Fe corrosion, metallic Fe is oxidized to Fe^{2+} serving as the anode and H_2O and O_2 react to form OH^- ions driving the reduction reaction serving as the cathode, forming surface adsorbed and dissolved $Fe(OH)_2$ (equation 2). This process occurs at any aqueous electrolyte(liquid)/Fe interface. $Fe(OH)_2$ can be further oxidized into Fe_2O_3 as a result of exposure to atmospheric $O_2(g)$, as shown in equation 3.[22]

$$Fe^{2+}(aq) + 2OH^-(aq) \rightarrow Fe(OH)_2(s) \quad (1)$$

$$2Fe(s) + 2H_2O(l) + O_2\,(g) \rightarrow 2Fe(OH)_2(s) \quad (2)$$

$$4Fe(OH)_2(s) + O_2(g) \rightarrow 2Fe_2O_3(s) + 4H_2O(l) \quad (3)$$
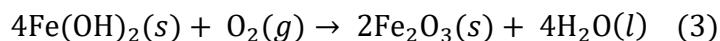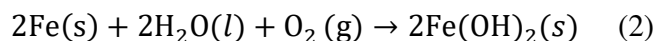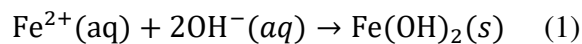
Also, under ambient conditions, atmospheric CO_2 can react with both $Fe(OH)_2$ and Fe_2O_3 to form $FeCO_3$ (siderite) as a secondary corrosion product at neutral and alkaline environment.[23] Also, it could lead to the formation of a mixture of Fe carbonate and hydroxide known as iron hydroxycarbonates.[24]

$$Fe_2O_3(s) + Fe(s) + 3CO_2(g) \rightarrow 3FeCO_3(s) \quad (4)$$

$$Fe(OH)_2(s) + CO_2(g) \rightarrow FeCO_3(s) + H_2O(l) \quad (5)$$

Our group has found that in aqueous solution, iron corrosion at the air/NaCl(aq)/Fe interface produces carbonate films from the adso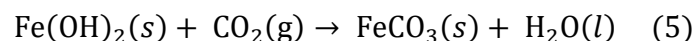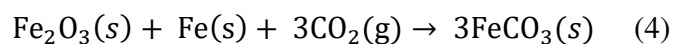rption of atmospheric CO_2 and O_2 using surface sensitive spectroscopic and microscopic techniques.[23] [18] Polarized modulated infrared reflection absorption spectroscopy (PM-IRRAS) was used to measure the influence of the electrolyte (NaCl(aq) or HCl(aq)) on the formation of mineral films.[23] The NaCl(aq) electrolyte provides an ion rich (Na^+ and Cl^-) and a semi-neutral environment to the air/liquid/Fe interface. The Cl^- ions are known to initiate the corrosion process through pitting. The electrolyte, NaCl(aq) catalyzes the corrosion process forming hydroxylated products at the air/liquid/Fe interface with the aid of atmospheric $O_2(g)$. Then this hydroxylated interface further reacts with atmospheric $CO_2(g)$ to produce a surface carbonate film, identified as siderite ($FeCO_3$) at the interface.[18, 23] The rate of corrosion and the composition of the surface species depends upon the chemical environment of the Fe.[25] For instance, lepidocrocite (γ-FeOOH) is the main corrosion product under an acidic (low pH) environment and a mixture of siderite ($FeCO_3$) and lepidocrocite are produced under a semi-neutral pH chemical environment.[23]

In this study, a surface science approach was used to investigate the initial stages of Fe surface corrosion at the gas/solid interface under controlled exposure of essential reactants of Fe corrosion, O_2 gas, H_2O vapor, and ions. As corrosion is an electrochemical redox process, where the iron surface serves as the anode driving the anodic oxidation reaction, while water and O_2 drives the cathodic reduction reaction. This study utilized two separate experiments to study the effect of the reactants, H_2O and O_2, on the corrosion of iron in the presence of NaCl. The first part varies the ratios of O_2 and H_2O pressures of iron with NaCl to measure the surface species and oxidation states at the gas/solid interface using near ambient pressure X-ray photoelectron spectroscopy (NAP-XPS). The second experiment separated the H_2O and O_2 reactants to measure the effect of each on the surface carbonation using *in situ* PM-IRRAS and Auger electron spectroscopy (AES). This investigation measured the synergistic effect of water and oxygen on the oxidation mechanism leading to corrosion. The composition of surface and a proposed mechanism is presented for the formation of carbonate films through surface oxidation processes.

2.0 Experimental materials and methods

2.1 Sample preparation

An Fe foil (Iron II, 99.99%, Allied Metal Corp.) sample was polished as described previously to obtain a mirror finish.[23] The sample was machined to a size of 1 cm × 1 cm. Both sides of the sample were polished with using sandpaper with grit sizes 400, 600, 800 and 1200 at Michigan Technological University. The final stage of polishing was completed by using polishing pads with 0.05 μm colloidal silica suspension to get a mirror finish. The polished sample was cleaned with Micrell soap water, rinsed in nanopure water, sonicated in ethanol, and dried in air.[23]

2.2 NAP-XPS analysis: The NAP-XPS experiments were conducted at beamline 9.3.2 end station at the Advanced Light Source (ALS) at Lawrence Berkeley National Laboratory (LBNL). The polished Fe sample was first mounted to a sample holder using carbon tape and copper clips with a thermocouple underneath the sample. The Fe surface loaded into a vacuum chamber and transferred into a process chamber equipped with an ion gun for Argon sputtering. The sample was

Ar$^+$ sputtered under 1.5 keV and 15 mA current at 1×10^{-5} torr pressure for 40 minutes. These conditions were found to remove carbon from iron oxide surfaces.[26, 27] Next the sample was removed and placed in a glove box filled with nitrogen. A droplet of 10 mM NaCl(aq) was placed on the Fe sample and dried until a white film was observed, as shown in Figure 1A-C. Next the sample was placed back into the vacuum chamber, through a nitrogen-filled glove bag, and transferred into the analysis chamber with a base pressure of 5×10^{-9} Torr.
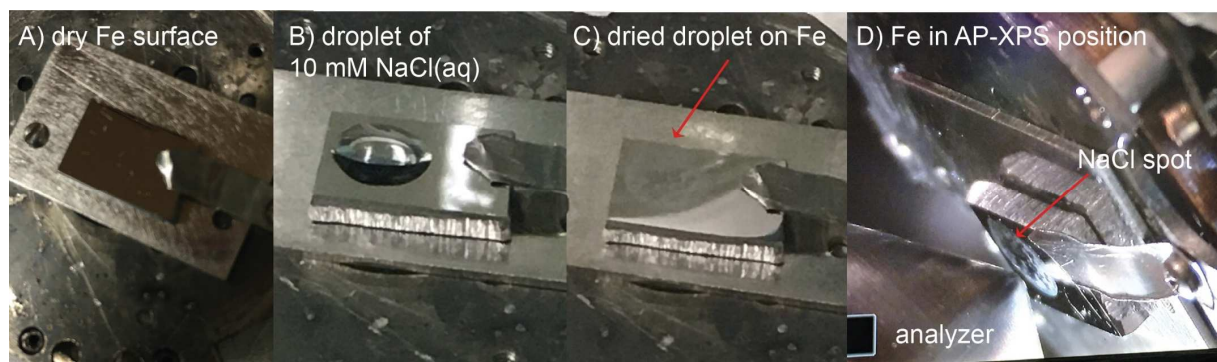

Figure 1: A) The polished Fe sample mounted to the sample holder. B) A droplet of 10 mM NaCl was C) dried on the sample in a nitrogen glove box. D) The spot on the Fe sample placed in front of the analyzer aperture in the AP-XPS analytical chamber

The sample distance from the analyzer was set to 800 μm. The angle between photon beam and the analyzer was 70⁰ while the analyzer was oriented normal to the surface, as shown in Figure 1D. Therefore, the angle between the polarization vector and photoelectron direction was 20⁰. The distance between Si$_3$N$_4$ window and the sample was 10 cm. NAP-XPS spectra of the C 1s (hv = 535 eV), O 1s (hv = 780 eV), Cl 2p (hv = 448 eV), and Na 2s (hv = 314 eV) regions were collected at a kinetic energy of 250 eV. The Fe 2p (hv = 850 eV) region was collected at a kinetic energy of 140 eV. The flux was estimated from the beam current, I_o at each photon energy.

The NAP-XPS of the C 1s, O 1s, Na 2s, Cl 2p, and Fe 2p regions were collected on the dried NaCl spot and a spot of the clean Fe surface with no NaCl. To assess the effect of the key reactants of H_2O and O_2 on the iron surface oxidation, different partial pressures were co-dosed to expose the sample to different ratios of H_2O and O_2. The stoichiometric ratio between H_2O and O_2 is 2:1, as shown in equation 2. Therefore, when the NAP-XPS experiment was being conducted, the water pressure was maintained inside the analytical chamber at 100 mTorr and gradually increased the O_2 pressure. According to equation 2, at optimum stoichiometric ratio (2:1), the H_2O and O_2 pressures are 100 mTorr (H_2O):50 mTorr O_2. Because all the NAP-XPS experiments were conducted at isothermal (T = 298.15 K) conditions, it is assumed that pressure ratios of gasses represent their molar ratios. Also the pressure of O_2(g) was further increased until the pressure ratio became 1:1 for H_2O and O_2 to study whether further changes occurred on the surface. This allowed for monitoring the initial stages of Fe oxidation at gas/Fe interface.

The spectra were collected on the dried NaCl spot in two stages. Stage 1: variation of O_2 pressure at constant pressure of 100 mTorr of water vapor i) the initial spectra in ultra-high vacuum (UHV) conditions, ii) 100 mTorr H_2O pressure, iii) 10 mTorr O_2 pressure and 100 mTorr H_2O constant

5

pressure, iv) 50 mTorr O_2 pressure and 100 mTorr H_2O constant pressure, v) 100 mTorr O_2 pressure and 100 mTorr H_2O constant pressure and, vi) UHV conditions. Stage 2 was collected by variable dosing of O_2 pressure with no water vapor: i) in UHV, ii) 10 mTorr of O_2 pressure, iii) 50 mTorr of O_2 pressure, iv) 100 mTorr of O_2 pressure and, v) the final spectrum in UHV conditions.

2.3 NAP-XPS Data analysis: The high-resolution spectra of each region were fitted into different chemical species using CasaXPS software applying the Shirley background and a 100% Gaussian line shape. To compare the elemental ratio and changes in chemical species on the NaCl spot on Fe as a function of O_2 and H_2O pressure, areas of each chemical species found in each XPS region were corrected using normalization factors. The normalization factors (Nf) were calculated for each XPS region separately using the relationship; Nf = Transmission × Flux × cross sectional factor defined in Yeh and Lindau.[28] The transmission of photoelectrons were extrapolated within $10 - 900$ eV photon energy according to each pressures of O_2 and H_2O using the gas transmission database of the center for X-Ray optics at Lawrence Berkeley National Laboratory's (LBNL) materials sciences division.[29] The flux of the photon beam at each photon energy were extrapolated using the flux-photon energy. The cross sectional factor for each orbital were calculated using the atomic subshell photoionization cross sections and asymmetry parameters.[28] The photo ionization cross sections and asymmetry parameter, β, were used from the published tables from the Elettra and Fermi light sources as a function of photon energy. The angle between polarization vector and photoelectron direction, γ was set at 20⁰. All the XPS fitted peak areas were corrected by dividing the normalization factors for each high-resolution region. All the areas were then normalized to the area of total Fe 2p area to obtain the relative elemental ratio of the species on the surface at different experimental conditions. For the simplification, the analyzer transmission function was assumed to be a constant, as spectra were collected at the same 250 eV kinetic energy. The Fe 2p region was collected at 140 eV KE, due to the limited photon energy range at beamline 9.3.2.

2.4 *Ex situ* XPS analysis: After the NAP-XPS experiments, the sample was reanalyzed using laboratory-based XPS instrument (PHI 5800 XPS instrument, Perkin Elmer, Physical Electronics model) at Michigan Technological University ACMAL facilities to investigate the post oxidation on metallic Fe, after two days of exposure to atmospheric air. The spot with the NaCl droplet and the clean iron area were scanned to assess the C 1s, O 1s, Na 2s, Cl 2p and Fe 2p regions. A Mg anode operated at 1253.6 eV photon energy at 15 kV and 400 W, with a 800 μm diameter spot size. Survey spectra were collected using a pass energy of 187.85 eV, step voltage of 0.8 eV, and a dwell time of 20 ms/step. The high-resolution spectra of the C 1s, O 1s, Na 2s, Cl 2p and Fe 2p regions were collected using a pass energy of 23.50 eV, step voltage of 0.1 eV, and a dwell time of 100 ms/step. The peak deconvolution of high-resolution spectra was performed using CasaXPS software applying Shirley background and 100% Gaussian line shape.

2.5 Polarized modulated-infrared reflection absorption spectroscopy (PM-IRRAS) experiments

Sample cleaning, PM-IRRAS, and AES were performed in custom-designed surface analysis chamber with a base pressure of $1\text{x}10^{-9}$ Torr, in the Perrine research lab at Michigan Technological University. A separate Fe sample was polished and cleaned, as described above. The sample was

mounted to a custom-designed sample holder constructed with copper connectors, held in place between two Tungsten wires, used as a resistive heater, and secured with tantalum foil clips. A K-type thermocouple was tightly sandwiched between the iron sample and a graphite sample (used as a backing material). The copper sample holder was secured to a motorized xyz manipulator (McAllister Technical Services) with a 500 mm z-travel distance and a differentially pumped 360 ° rotary platform.

The Fe sample was sputtered with argon gas (99.999% purity, American Welding and Gas) at a pressure of 5×10^{-5} Torr at 1 keV for 30-45 minutes using an ion gun (IG2, RBD Instruments) at an angle of 54 degrees with respect to the surface plane. After sputtering, the sample was annealed at 500°C for 10 minutes at a base pressure of 2×10^{-9} Torr. The surface elemental composition and cleanliness were measured using Auger electron spectroscopy. Next, the sample was moved to a reactor chamber (custom design, Kimball Physics), mounted with ZnSe windows for PM-IRRAS measurements. A ThermoScientific iS50R FTIR instrument was used to produce a broadband infrared light with KBr windows and a KBr beamsplitter. The light exited the bench instrument, reflected off of a flat aluminum mirror, an aluminum parabolic mirror, through a photoelastic modulator (PEM, Hinds, Inc.) with a ZnSe coating, and focused onto the mounted Fe sample inside the UHV surface analysis chamber. After a single reflection, the reflected light was refocused onto a MCTA detector that was cooled with liquid nitrogen. PM-IRRAS measurements were collected at a grazing angle of 82 degrees using 1000 scans, 4.0 cm^{-1} resolution, gain of 8.0, which produced a p/p interferogram signal of 2.34-2.40.

First, water vapor (nanopure water) was dosed through a variable leak valve in units of Langmuirs (1L = 1×10^{-6} Torr· second) of exposures of 0.5, 1.0, 10, 88.5, 900 L. Next, oxygen gas (99.999%, American Welding and Gas) was exposed to the sample in the same exposures as the water vapor. PM-IRRAS spectra were collected after each vapor or gas exposure. No apparent reflection modes were observed in the PM-IRRAS spectra. Afterwards, the sample was Ar^+ sputtered and annealed prior to removing the sample through a load lock chamber, at a base pressure of 2×10^{-8} Torr. The sample, still mounted on the removable sample holder, was placed in a plastic bag backfilled with a positive pressure of nitrogen gas (99.999%, American Welding and Gas). A 10 mM droplet of NaCl(aq) was placed on the sample and allowed to dry in the nitrogen-filled glove bag. After the droplet was dried, the sample holder was transferred through the glove bag into the load lock chamber and pumped for 2.5 hours to a pressure of 5×10^{-7} Torr, to minimize exposure to ambient air to prevent surface oxidation. The sample was then transferred to the main chamber, base pressure of 1.7×10^{-9} Torr. AES was immediately collected on the sample at three different spots.

The sample was then moved to the reactor chamber for PM-IRRAS measurements, first exposing it to H_2O vapor with increasing exposures (in units of Langmuirs): 0.5, 1.0, 10, 88.5, 900 L and then the same exposures for O_2. Next, the reactor was isolated from the main chamber using a UHV gate valve (VAT). O_2 gas was exposed to the sample through the leak valve to near ambient pressures (10s of millitorr) as measured using a Baratron vacuum gauge. The pressure in the reactor was throttled through a 2nd gate valve (VAT) through a hybrid turbomolecular pump (Pfeiffer, Inc.).

The PM-IRRAS data was baseline corrected by subtracting the initial spectrum after the exposure to the 10 mM NaCl droplet from all the subsequent spectra. The peak area of the carbonate stretching mode (νCO_3) was integrated and plotted as a function of Langmuirs. A first order kinetics equation was used to fit the data and the Langmuir adsorption isotherm model was used to fit the near ambient pressure XPS data.

2.6 Auger electron spectroscopy (AES) measurements

A mini-cylindrical mirror analyzer (mini-CMA) oriented 90 degrees from a low energy electron diffraction (LEED) (LK Technologies, Inc.). The LEED instrument is equipped with an electron gun, where the gun energy was set at 1.5 keV for AES measurements. The CMA distance is adjustable and was within 0.5 inch from the sample. The sample was oriented at 19 degrees with respect to the CMA analyzer to eject electrons into the CMA detector. AES spectra was collected at a scan rate of 1.0 V/channel, 0.1 seconds/channel with 3-5 sweeps. Three separate spots were analyzed between sputtering and annealing cycles, and after PM-IRRAS experiments to check for reproducibility.

3.0 Results and discussion

3.1 NAP-XPS in H_2O vapor and O_2 gas

The collection of *in situ* NAP-XPS spectra of the gas/solid interface on the NaCl spot deposited on the iron surface was conducted in two stages. In the first stage, O_2 pressure was increased from 0 mTorr to 100 mTorr stepwise, while holding the H_2O pressure inside the analytical chamber at a constant pressure of 100 mTorr. XPS spectra were collected at every pressure until a O_2:H_2O ratio of 1:1 was achieved. This was to measure the effect of the stoichiometric ratio of O_2 and H_2O, two of the key reactants in the first two redox steps of the corrosion reaction on iron, as shown in equation 2. The O_2(g) pressure was gradually increased at a constant water vapor pressure and increased the O_2(g) pressure until the system roughly reached a 1:2 ratio and further increased the O_2(g) to check whether further changes occurred at a 1:1 ratio. The NAP-XPS spectra of C 1s, O 1s, Na 2s, Cl 2p and Fe 2p regions were collected on the NaCl spot dried on the iron surface in comparison to the clean iron surface without NaCl.

The NAP-XPS spectra of the fitted C 1s, O 1s and Cl 2p regions are shown in Figure 2A-C. The initial spectra for each region are shown in the supplemental information in Figure S4. The O 1s region of the NaCl spot shows a peak at 529.2 eV in Figure 2A, which can be assigned to oxidized iron (Fe-O). A second peak at 531.8 eV represents various types of surface species that overlap at the same binding energy: both surface hydroxyl species, from the hydroxides (Fe(OH)$_2$), oxyhydroxides (FeOOH), and carbonates (Fe-OH/CO$_3$). This peak area is larger in the NAP-XPS experiments owing to its high surface sensitivity. These binding energies are close to each other and it is difficult to resolve peaks for each species.[30] The intensity of the peak at 531.8 eV is also observed to gradually increase as O_2 pressure increases at a constant H_2O vapor pressure of 100 mTorr. This suggests that both hydroxylation of the iron surface and carbonation increases as the H_2O:O_2 ratio increases. After the complete evacuation of O_2(g) and water and regenerating the

8

vacuum, the intensity of Fe-OH/CO$_3$ peak at 531.5 eV in the O 1s region remains at the highest value, indicating the Fe-OH/CO$_3$ species is stable and that the surface is oxidized.
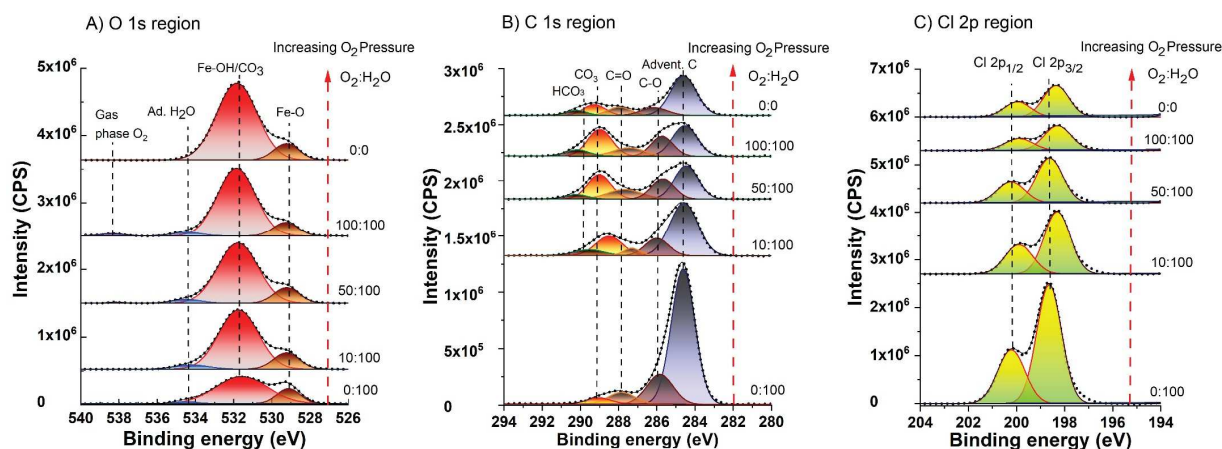

Figure 2: The O 1s, C 1s and Cl 2p regions of the Fe surface with dried NaCl. As O$_2$ pressure increases from 0 to 100 mTorr at 100 mTorr constant H$_2$O pressure, adventitious carbon decreases and surface CO$_3$ increases, and Fe-OH are formed. The Cl$^-$ intensities decrease with increasing O$_2$ pressure.

In the C 1s region in Figure 2B, there are four peaks on the spot of the dried NaCl droplet resulting from minor contaminants from either the 10 mM NaCl(aq) solution or minor exposure to pumping gases during the sample transfer into the UHV analysis instrument: 284.6 eV (adventitious C), 285.8 eV (C-O), 287.8 eV (C=O), 288.5 eV (CO$_3$), and 290.2 eV (HCO$_3$). The intensity of the adventitious carbon peak is shown to decrease, at the same time, the intensity of the carbonate peak at 289.0 eV gradually increases. This observation indicates that the adventitious carbon on iron (NaCl spot) is oxidized and transformed into surface carbonate species (CO$_3$ and HCO$_3$). At the initial UHV condition at a pressure of 3.1×10^{-9} Torr, there was only a small amount of residual carbonate, and no bicarbonates present on the surface. This suggests that adventitious carbon on the iron surface (which are mainly found on any surface as hydrocarbon contaminants) are oxidized in O$_2$ and correlates with the increase in surface CO$_3$ and HCO$_3$.

The Cl 2p region in Figure 2C panel shows both the Cl 2p$_{3/2}$ and Cl 2p$_{1/2}$ peaks with a primary binding energy of the Cl 2p$_{3/2}$ peak between 198.3-198.6 eV, assigned to the Cl-Na species. The Cl 2p peak intensities were observed to decrease when the O$_2$ gas pressure increased at constant H$_2$O pressure of 100 mTorr. It is known that the Cl$^-$ penetrates into the native oxide layer pitting the Fe surface during the initial stages of corrosion.[31] [32] This suggests that the decrease of the intensity of Cl 2p region may due to the adsorption of the Cl$^-$ anions from the NaCl spot into the underlying surface. A second peak was observed at binding energies between 192.1-192.5 eV, as shown in supplemental figures S1 and S4. Its origin is likely due to boron impurity on the iron surface. With increasing O$_2$ exposures, the boron oxide peak area also increases and remains stable after the chamber is returned to UHV pressures.

Stage 2 of the experiment was carried out with increasing O_2 gas pressure and no exposure to H_2O vapor (0 mTorr). The NAP-XPS spectra and fittings of the C 1s, O 1s and Cl 2p regions are shown in Figure 3. No significant new changes are observed of either surface composition or concentration, after the exposures of H_2O and O_2 from stage 1. In the C 1s region, there is a slight decrease in the adventitious carbon (C-H) peak area at 284.6 eV and a slight increment in the carbonate and bicarbonate peaks at 289.0 eV and 290.9 eV, respectively as the O_2 pressure increases. This suggests that oxidation occurs slowly on the surface or simply due to the oxidation of adventitious C into carbonates which only requires O_2 gas. Similarly, there is little change in the amount of the chemical species in the O 1s and Cl 2p regions. There could be two possible reasons for this observation. First, one of the essential reactants of corrosion, H_2O, is absent as the reactant, which was not dosed in the stage 2. Secondly, surface oxidation in corrosion is irreversible and may explain the lack of changes resulting from stage 1 is irreversible. If the corrosion of the NaCl spot is completed, there would only be a slight further oxidation. The reason is, there may be a thin adsorbed H_2O layer on the NaCl spot on the iron surface from the stage 1 of the corrosion experiment. Even though, at UHV conditions (3.1×10^{-9} Torr) the UHV conditions were regenerated before starting stage 2, it is difficult to completely remove the adsorbed H_2O layer. Therefore, the adsorbed thin H_2O layer may contribute to the slow oxidation on the surface.
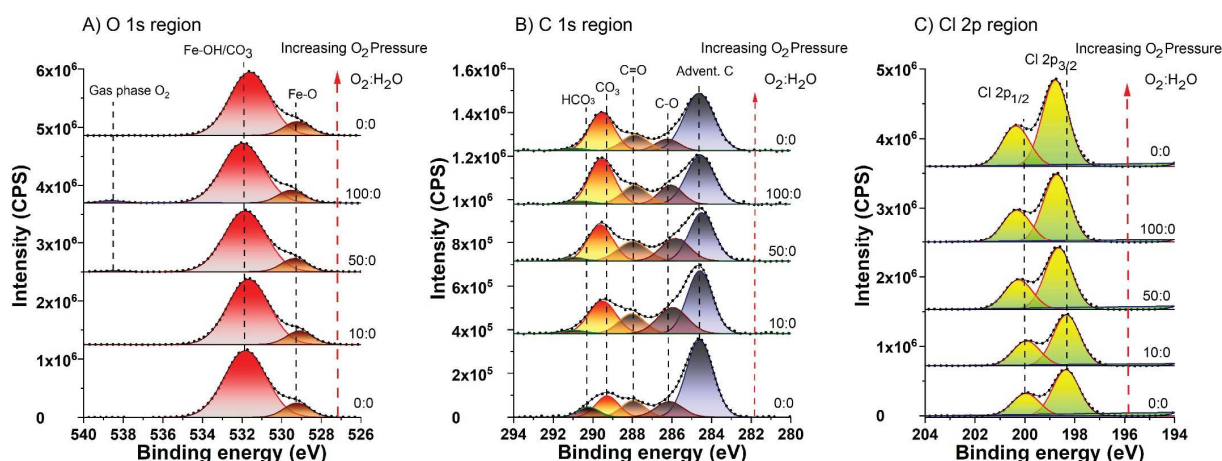

Figure 3: The O 1s, C 1s and Cl 2p regions of the Fe surface with dried NaCl. As O_2 pressure increases from 0 to 100 mTorr, the peak area intensities for the surface remain the same Further surface oxidation and adsorption are minimized without the presence of water vapor.

The Cl 2p region shows no significant shifts in binding energies as O_2 pressure increases from 10 mTorr to 100 mTorr at 0 mTorr of H_2O vapor. Although the Cl 2p intensity appears to increase slightly, no other changes were observed. This suggests that the same amount of Cl^- ions exist on the surface of iron (NaCl spot) when O_2 pressure increases alone with no H_2O dosing into the system. This observation is different to what was observed in the stage 1 of the corrosion experiment where both O_2 and H_2O were available, the Cl 2p intensities decrease. The boron oxide peak at 192.3 eV remains at the same concentration during exposure to only O_2.

The Fe 2p and Na 2s regions were also assessed along with the C 1s, O 1s, and Cl 2p regions. The presence of Fe^{2+} was observed in the $Fe2p_{3/2}$ region at 710 eV with iron oxide species at 713.4-714 eV. The Na 2s binding energy was observed between 63.2-63.6 eV and assigned to the Na-Cl species from the NaCl dried salt on the iron surface. No additional changes were observed in either stage 1 or stage 2 of H_2O and O_2 exposures suggesting that only the top layers of the surface are affected in the O 1s, C 1s, and Cl 2p regions. Details and spectra for the Fe 2p and Na 2s are given in Figures S1 and S2 in the supporting information, respectively.

3.2 *Ex situ* XPS analysis

The same Fe sample was re-analyzed using *ex situ* XPS to assess the effect of (2 days) exposure of ambient conditions after the *in situ* NAP-XPS to measure the stability of the carbonate species. Details of the scanning parameters are described in the experimental methods section. The spectra from the O 1s, C 1s, Cl 2p, Fe 2p, and Na 2s regions are given in the supporting information section in comparison to the initial Fe surface prior to H_2O and O_2 exposures from the NAP-XPS experiments in Figure S2-S4 in the SI section.

To give a summary, after exposure to ambient conditions for two days, the largest species present in the C 1s region was adventitious carbon. The CO_3 and HCO_3 species, produced from the NAP-XPS experiments, are still present as well as the $FeOH/FeCO_3$ species in the O1s region. Because the adventitious carbon has been deposited on the surface, CO_3 and HCO_3 species have become minor components on the sample surface relative to adventitious carbon peak intensity. Also, the *ex situ* XPS analysis confirmed the final products of iron corrosion as iron oxides and carbonates, confirming their stability on the surface. The intensities from the adsorbed Cl^- species decreased in the Cl 2p region and the boron oxide peak at 191.5 eV is not observed in the *ex situ* XPS analysis (see Figure S4). The peak area decreased significantly and the minor peak area present at 190.7 eV has been observed previously in our other samples exposed to metal chloride salt solutions (unpublished). This peak area in the *ex situ* XPS is attributed to X-ray satellites originating from non-monochromatic sources from non-principle photons. In the NAP-XPS experiments, the presence of boron oxide was measured on the bare iron surface with no NaCl and is from the minor impurity, intrinsic to the iron substrate. Since it is only present in the NAP-XPS experiments, this suggests that the boron oxide becomes apparent near the top layers of the surface. Further details of the *ex situ* XPS spectra are given in the SI section.

3.3 Area calculations of different photo spectroscopic regions

To further understand the initial stages of surface corrosion, the peak areas of select surface species were normalized to the Fe 2p total peak area to obtain the elemental peak area ratios and plotted as a function of O_2 gas pressure. Figures 4 and 5A show the peak area ratios of chemical species from the C1s and O1s regions and the Cl 2p region, respectively of the NAP-XPS spectra for both stage 1 and stage 2 of the corrosion experiment.

Figure 4A shows a decrease in the adventitious carbon and Figure 4B shows a corollary increase in surface carbonates with increasing O_2 gas pressure at a constant 100 mTorr of H_2O vapor (red

11

squares). After the pressure is returned to UHV conditions (filled in red squares), the adventitious carbon remains low on the surface and surface adsorbed carbonate has increased. This suggests that the adventitious carbon on the iron surface is oxidized in H_2O and O_2 to form surface carbonate as one of the corrosion products. In comparison to the clean Fe spot with no NaCl (black triangles), the adventitious carbon and surface carbonates remain at similar ratios. A similar trend is observed in Figures 4C-D that compare the total O1s peak area/Fe2p area ratio and the O1s ($FeOH/FeCO_3$)/Fe 2p ratio, where the surface is clearly oxidized in the presence of O_2 and H_2O on the Fe surface with the NaCl resulting in the formation of adsorbed carbonates (red squares) compared to the clean Fe surface (black triangles).

In stage 2, where there was no partial pressure of H_2O present during O_2 exposure, no change in adventitious carbon or surface carbonates are observed (blue circles). This may be due to the fact that the NaCl spot was used for stage 1 and the surface of NaCl spot already had a significant amount of corrosion products, where the oxidation is irreversible. If that spot is already saturated with carbonates or if most of the adventitious carbons were already oxidized into carbonates, no change in the peak area ratios is expected. Also, H_2O was not dosed in the stage 2, which is an essential reactant for iron corrosion. However, the fact that the surface is still slowly oxidizing may be attributed to the fact that the NaCl spot contains a thin layer of trapped H_2O allowing for slow oxidation to continue. The corollary peak area ratios from the *ex situ* XPS experiment are shown for comparison (green pentagons). These show that the adventitious carbon remains low, albeit with a beam energy of 1253.6 eV (KE = 530 eV for the O1s region) from the Mg anode that probes much deeper (> 3-5 nm) compared to the < 1.2 nm 250 eV kinetic energy from the NAP-XPS experiments. These results suggest the adsorbed carbonates remain stable on the surface after ambient air exposure of H_2O and O_2.
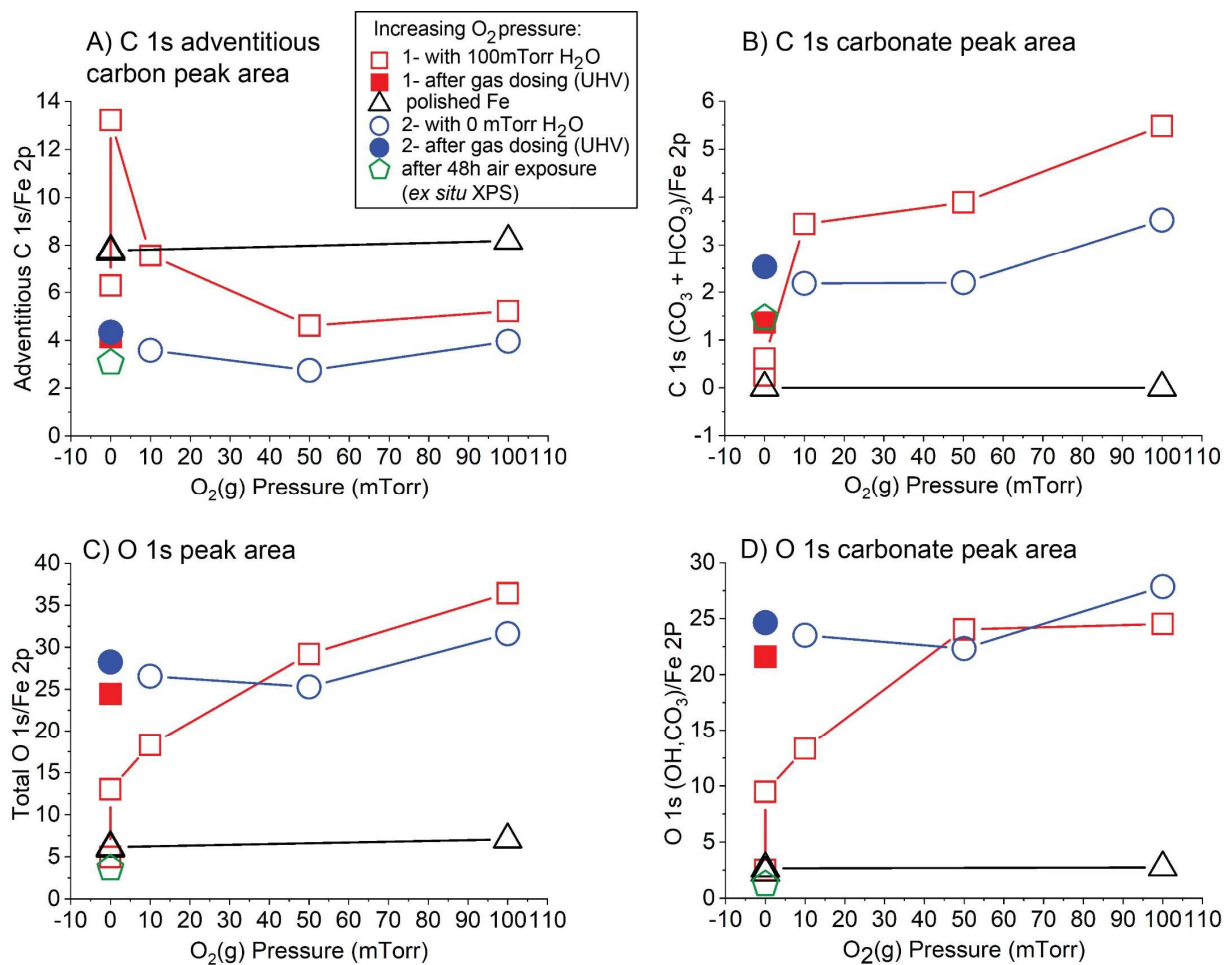
Figure 4: Variation of normalized areas of adventitious and carbonate peaks of C 1s regions as a function of O_2 gas pressure in stage 1 and stage 2 of NAP-XPS corrosion experiment. Markers: red squares stage 1 dosing both O_2 and H_2O, blue circles – stage 2 dosing only O_2, black triangles – stage 1 on polished iron with no NaCl, green pentagons – *ex situ* XPS after 2 days of air exposure, filled in markers are the data after returning the pressures to UHV pressures.

We can also account for other sources of carbonates that may or may not be contributing to the growth of surface carbonates. The adventitious carbon on iron at the initial UHV conditions is less than the amount of adventitious carbon detected at 0 mTorr of O_2/100 mTorr water and 10 mTorr of O_2/100 mTorr of water. This may be due to the residual hydrocarbons in gas phase that was present during the initial doses of water from the gas lines and are adsorbed on the surface.[33] Mass spectrometry data, shown in Figure S5 in the SI section, collected during the NAP-XPS experiment show little presence of CO or CO_2 during near ambient pressure exposures. Additionally, as the O_2 pressure increases, the amount of adventitious carbon decreases indicating that oxidation at the end of the experiment is less. Therefore, the overall amount of adventitious carbon has decreased due to oxidation by H_2O and O_2.

When the surface hydrocarbons are oxidized and form surface adsorbed carbonate, the process is irreversible and when the reaction chamber is returned to UHV conditions, the carbonates on the

13

surface remain constant. Possible errors in the marker at a 1:1 ratio of $H_2O:O_2$ compared to the marker in UHV conditions (filled in circles) is that surface carbonates may be soluble in the adsorbed water layer on the NaCl spot (on iron) forming gas phase CO_2 or $CO_3^{2-}/HCO_3^-/H_2CO_3$, which may be pumped away along with water when the UHV was regenerated. However, no evidence of gas phase carbonates was observed in the mass spectra collected during the experiment. This may be why a slight reduction in CO_3 ratios at UHV conditions is observed.

The behavior of Na^+ and Cl^- ions on the NaCl spot was also assessed using the Cl 2p and Na 2s regions. The Cl 2p/Fe 2p and the Cl 2p/Na 2s elemental ratios were calculated and plotted as a function of O_2 gas pressure for both stage 1 and stage 2, shown in Figure 5A and 5B, respectively. Figure 5A shows that the relative Cl^- concentration decreases with increasing O_2 pressure at a constant 100 mTorr of H_2O vapor (red squares). After returning the pressure to UHV conditions (filled in red squares), the relative Cl^- concentration remains the same. However, small shifts in binding energy were observed, shown in Figure 2C or 3C suggesting that slight changes in the chemical environment of the Cl^- anion and Na^+ cation were produced (shown in Figure S6 in the supporting information). The clean Fe surface with no NaCl (black triangles) is shown as the control experiment, as expected. According to Figure 5B, the Cl^-/Na^+ ratio gradually decreases as the O_2 pressure increased at constant H_2O vapor pressure (red squares). This indicates that the amount of Cl^- on the surface is decreasing relative to the amount of Na^+ on the surface. Initially, the amount of Cl^- and Na^+ remain the same stoichiometry of 1:1 in NaCl, as shown as the initial data point and in the *ex situ* XPS data (green pentagons). But when the O_2 pressure is increased from 10 mTorr to 100 mTorr, the Cl^-/Na^+ ratio decreased from a ratio of 1.2 to 0.2, indicating that the amount of Cl^- has decreased on the surface by five times. The ratio remains constant after regenerating the UHV (filled in red squares). In stage 2, with no water vapor (blue circles), the relative Cl^- concentration remains low showing that the change is irreversible, as the Cl^-/Na^+ ratio does not undergo a significant change throughout the gas phase oxidation. These observations indicate that Cl^- ions move away from the surface but Na^+ remain on the surface when water is present (stage 1). However only when O_2 is present (stage 2), Cl^- ions ratio remains constant suggesting the requirement of H_2O for the Cl^- subsurface migration process (blue circles). For comparison, the *ex situ* XPS analysis (green pentagons) show that the Cl^- ions remain low, however because the penetration depth is much deeper, the Cl/Na peak area appears at the original 1:1 ratio.

The Cl $2p_{3/2}$ and Na 2s binding energies undergo small changes, up to +/- 0.4 eV from the exposure to oxygen and water vapor as shown in the Supporting Information in Figure S6. The Cl^- ion is already at a higher binding energy at 199.0 eV in the solution after it is applied to the iron surface prior to NAP-XPS and PM-IRRAS experiments. This is likely due to the interaction with the iron surface, as previously observed.[18] Upon exposure to water vapor and increasing O_2 the binding energy decreases by 0.4 eV, suggesting the Cl^- ion becomes hydrated or changes in the surface alter the Cl^- chemical environment. A similar trend is observed for the Na 2s binding energies, beginning at 64.0 eV and shifting lower by 0.76 eV. These small shifts in the binding energy should be interpreted with caution and may be due to a difference of charge correction, as these shifts are less than the energy resolution, < 0.50 eV. Further details of the binding energy shifts are given the Supporting Information.

The peak area analysis conveys that H_2O is required for separation of Na^+ and Cl^- in NaCl and the penetration or adsorption of Cl^- ions into the iron surface. We believe that H_2O is required to rehydrate the NaCl at which Na^+ ions and Cl^- ions are separated and obtain some mobility. Then as the O_2 pressure increases, Cl^- ions moves away from the analysis region and either adsorbs on iron surface or penetrates into the native oxide/iron surface. This resembles the physical mechanism of Cl^- ions, where Cl^- initiates corrosion by pitting into the native oxide layer.[2] However, because H_2O is not available in the stage 2 of corrosion experiment, NaCl becomes dehydrated, and Cl^- and Na^+ remain at the same ratio. These results suggest a synergistic effect of both H_2O and O_2 on the surface oxidation of hydrocarbons to carbonates. Valence band spectra is shown in the supporting information in Figure S10 that reflects changes in the oxidation in the O 2s and Cl 3p regions. Further studies below detail the individual influence of H_2O and O_2 on the iron surface oxidation.
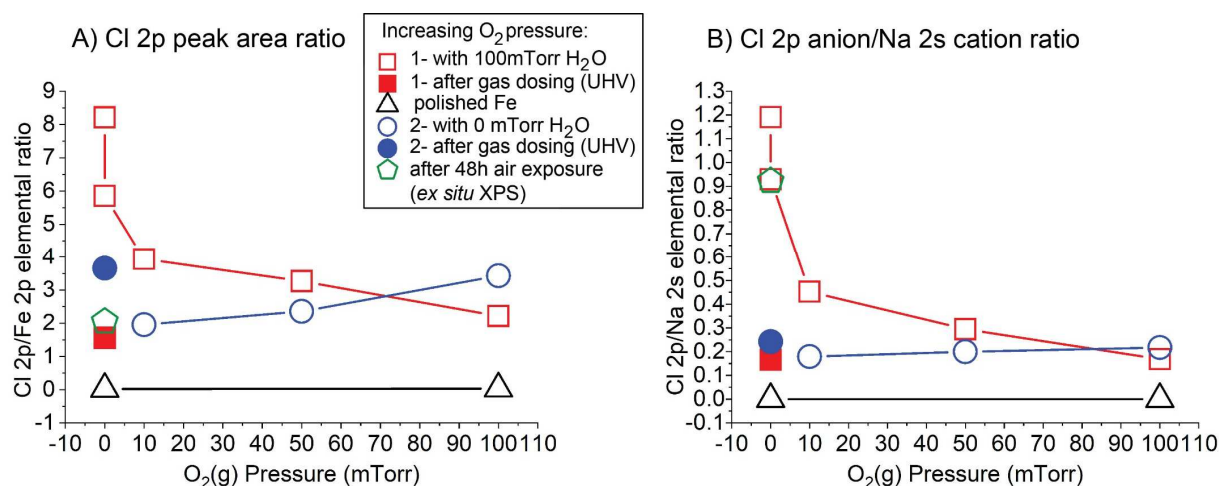

Figure 5: A) Area of the Cl 2p area normalized to Fe 2p and B) Area ratio of Cl^-/Na^+ of NaCl on iron surface as a function of O_2 gas pressure. Results suggest the Cl^- ions are moving into the subsurface region during oxidation in H_2O and O_2. Markers: red squares stage 1 dosing both O_2 and H_2O, blue circles – stage 2 dosing only O_2, black triangles – stage 1 on polished iron with no NaCl, green pentagons – *ex situ* XPS after 2 days of air exposure, filled in markers are the data after returning the pressures to UHV pressures.

3.4 Assessment of H_2O vapor and O_2 gas separately on iron oxidation using PM-IRRAS and AES

To investigate the initial stages of Fe surface oxidation in the presence of NaCl, *in situ* PM-IRRAS and Auger electron spectroscopy were used to measure the effect of H_2O and O_2 separately. First, an Fe sample with the dried droplet of 10 mM NaCl was prepared similarly to the sample used in the NAP-XPS experiments and then exposed to H_2O vapor in UHV, from 0.5 L to 1000 L. A PM-IRRAS spectrum was collected after every H_2O exposure. An Auger spectrum was collected to

check the surface chemical composition after the final water adsorption of the experiment. After dosing 1000 Langmuirs of water vapor, the sample was subsequently exposed to O_2 from 0.5 L to 1000 L. PM-IRRAS spectra were collected after every exposure. Afterwards, the O_2 pressure was increased and held at near ambient pressures (NAP) (70 mTorr, 100mTorr, and 120 mTorr) during collection of the PM-IRRAS spectra. Each spectrum took 8 minutes to acquire. Auger spectra was collected at the end of the experiment to check the final surface composition of the sample.

Figure 6A shows the 1800 cm^{-1} to 1000 cm^{-1} region of the difference PM-IRRAS spectra that were collected after each exposure of H_2O on the iron sample. A νCO_3 vibrational mode is shown to grow in at 1460 cm^{-1} after each H_2O exposure. It should be noted that this νCO_3 vibrational mode, along with reflectance modes at γCO_3 at 880 cm^{-1} and $\nu Fe-O$ at 670 cm^{-1}, were observed in the first spectrum. The data shown in Figure 6A is the difference of each spectrum subtracted from the initial spectrum, which shows the effect of water on the growth of the νCO_3 vibrational mode. Although water itself is not an oxidizing agent, the water exposures were shown to increase surface CO_3 formation, as shown in the inset in Figure 6A. The effect of O_2 exposure on the surface carbonation was also measured separately, after the water exposure, and results of the PM-IRRAS difference spectra are shown in Figure 6B, where the initial spectrum (before the water exposures) was subtracted from each spectrum. After O_2 exposure, the νCO_3 mode at 1460 cm^{-1} increased after O_2 exposures past 1000 L, as shown in the inset.
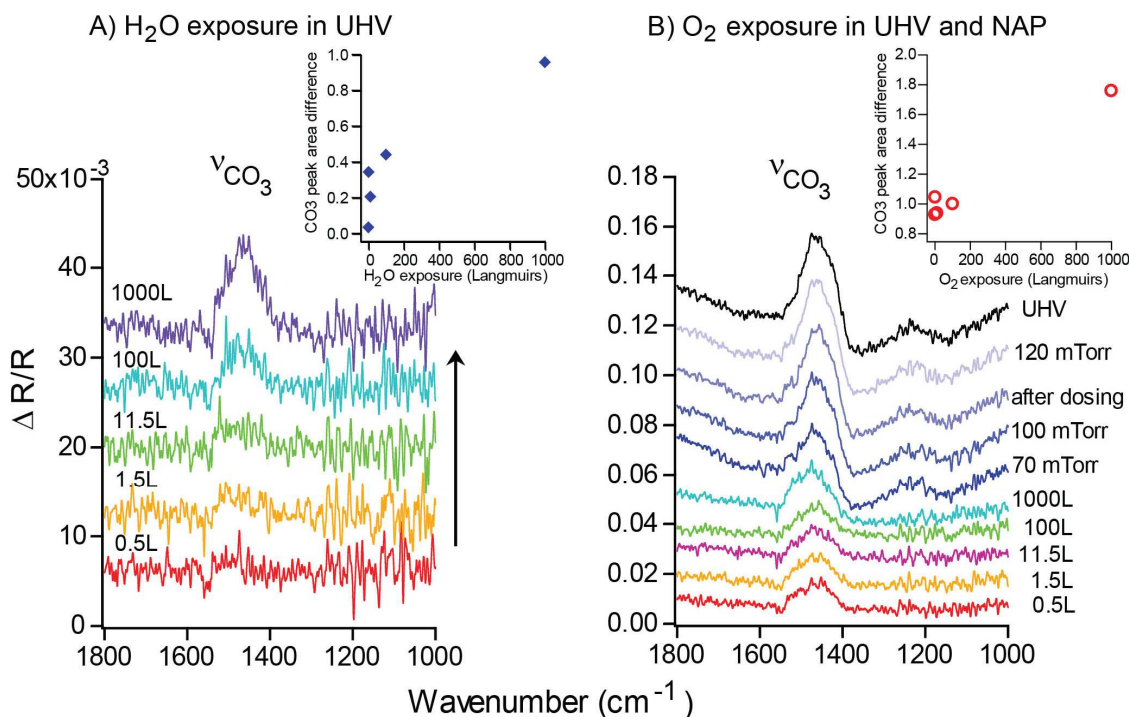

Figure 6: PM-IRRAS difference spectra from adsorption experiments of separate H_2O and O_2 exposure. A) Exposures (in Langmuirs) of water vapor or O_2 to iron with dried NaCl in UHV. The inset shows the adsorption for the CO_3 formation with H_2O exposure. B) Subsequent O_2 exposures

(in Langmuirs) and near ambient (NAP) pressures (in mTorr O_2). The inset shows the linear increase of the νCO_3 peak area difference as a function of O_2 exposure (in Langmuirs).

The inset in Figure 6A shows the growth of the νCO_3 vibrational mode that follows a 1st order kinetics. Using the νCO_3 peak area as coverage (θ) and the exposure (x in Langmuirs) as concentration, one can obtain the kinetic rate constant (k) for the formation of adsorbed carbonate using the following equation 6 for 1st order kinetics.

(6) $\qquad \ln(1 - \theta) = -kx$

This yields a rate constant of 3.92×10^{-3} L^{-1} for water adsorption. The activation energy can be obtained by converting the rate in units of L^{-1} to pressure using the conversion for exposure, where $1L = 1 \times 10^{-6}$ Torr·s. Assuming a pre-exponential factor 1×10^{13} s^{-1}, the activation energy is obtained as 93.6 kJ/mol for water. The data for O_2 exposures was also fit to equation 6, however the poor fitting suggested that there is little dependence of O_2 on the CO_3 growth at small exposures. This represents the growth of the carbonates are enhanced from the adsorption of water, but is probably catalyzed by the Fe site produced by NaCl corrosion of the surface. However, there are multiple steps from the conversion of hydrocarbons to carbonates, and one can only use this as an estimation of surface carbonate formation. A mechanism for this reaction is discussed below.

Upon exposure to near ambient pressures (NAP, from 70 mTorr to 120 mTorr) of O_2, where the O_2 is in equilibrium with the surface, the νCO_3 mode continued to grow at a linear rate, as shown in Figure S7C. These are compared to the adsorption experiments in the supporting information section in Figure S7in the supporting information. The final PM-IRRAS spectrum (UHV) was collected after returning the pressures to UHV conditions, below 1×10^{-8} Torr, showing that the carbonates remain on the iron surface.

These results from the PM-IRRAS experiments are contrasted to stage 1 of the NAP-XPS data, where O_2 was dosed at 100 mTorr of H_2O vapor. The NAP-XPS data was fitted using the Langmuir isotherm model, as the gas is in equilibrium with the surface, using the peak area coverage for the carbonate species in the C 1s and O 1s regions, shown in Figure S8 in the supporting information. To obtain the coverage, the total peak area of the carbonates (sum of the HCO_3 and CO_3 peak areas) were divided by the total C 1s peak area (total amount of carbon to be oxidized) in the initial C 1s or O 1s spectra prior to dosing H_2O or O_2. This resulted in the relative coverage of carbonates on the surface and was renormalized to a maximum coverage of 1.0. Both the data in the C 1s and O 1s regions showed the carbonates followed a first order adsorption kinetics. From the Langmuir adsorption model, the change Gibbs free energy was calculated assuming equilibrium, and was found to be -9.79 kJ/mol for the C1s region and -8.45 kJ/mol for the O1s region. Equilibrium constants were obtained and found to range between 51.9 for the C 1s region and 30.3 for the O 1s region. However, these energies are only an estimate of the Gibbs free energy for the synergistic effect of O_2 with H_2O vapor to produce carbonates from surface hydrocarbons. This means that the co-adsorption of the key reactants and several elementary steps should be considered for oxidation of the adventitious carbon to carbonates.

After each set of PM-IRRAS experiments, Auger spectra were collected before and after the H_2O and O_2 exposures, given in Figure 7. Figure 7A, shows the Auger spectrum collected on the clean Fe surface before starting the experiment with Fe as the major chemical component. Traces of other elements (C, O, and N) from surface contaminants, which can exist on the surface of Fe surface in small amount even after sputter cleaning annealing process due to the residual gases in the vacuum chamber. The Auger spectrum 7B represents the surface chemical composition of the dried NaCl spot deposited on Fe surface before dosing gases. This clearly shows a significant decrease in the Fe LVV Auger line and increased amounts of C KLL and O KLL signals on the surface. The carbon and oxygen signals may have been introduced onto the surface from the dried NaCl droplet from trace amounts of impurities. Other elements that are observed on the surface are the Cl LVV and Na KLL Auger lines, which are from the ions. Spectrum 7B of the dried NaCl droplet on the Fe surface is compared to spectrum 7C, which shows the spectrum after exposure to H_2O and O_2. After dosing 1000 L of H_2O and 1000 L of O_2 (spectrum 7C), the intensity of Fe LVV Auger line has decreased compared to the initial spectrum (spectrum 7B), due to surface oxidation. After dosing O_2 near ambient pressure conditions (spectrum 7D), the same phenomenon was observed for NAP-XPS experiment where Fe 2p signal has decreased after the surface oxidation.
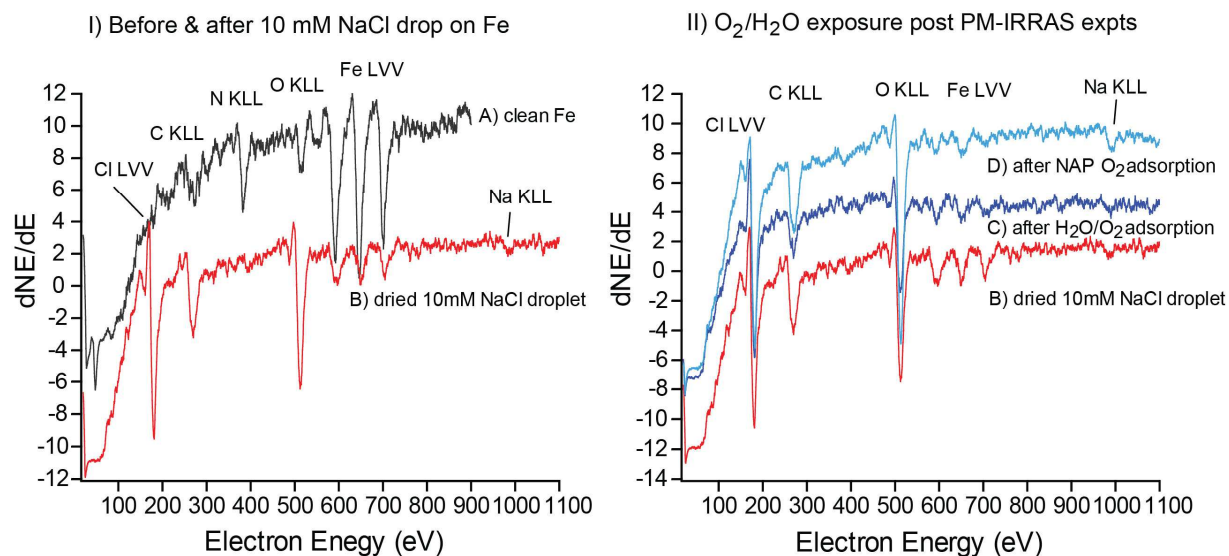

Figure 7: Auger electron spectroscopy measurements collected before and after PM-IRRAS experiments. A) Spectrum of the clean iron surface after sputter/annealing, B) the Fe surface after the 10 mM NaCl(aq) droplet was dried, C) spectrum B after exposure to H_2O and O_2 exposures, D) Spectrum C after exposure to near ambient pressure (NAP) O_2.

Table 1 compares the relevant elemental ratios from the Auger spectra in Figure 7. After H_2O and O_2 exposures, the relative amounts of oxygen and carbon have increased, whereas the Cl:Na ratio has decreased similar to the observations from the NAP-XPS experiments. According to Table 1, the O/Fe ratio has increased from 1.94 to 7.33 and the C/Fe ratio has increased from 2.39 to 5.79. It is also apparent that the oxygen content on the Fe sample surface increases due to the surface

oxidation upon exposure to O_2 and H_2O vapor. This may be attributed to the decrease in Fe LVV signal, thus raising the C/Fe ratio. Also it is possible some minor composition of the residual hydrocarbon species available in the vacuum chamber react with the surface or from the carbonate species, increasing the ratio to 5.79. Overall, the total increase in the O KLL signal from the gas phase oxidation of the surface, thus decreasing the C/O ratio to 0.79. The most interesting observation that corroborates NAP-XPS results is the decrease in Cl/Na ratio on the surface after dosing H_2O and O_2 from 2.90 to 2.42, and finally to 1.71 after exposure to NAP O_2. This supports our hypothesis that when the corrosion process occurs on the surface, Cl^- ions penetrate into the native iron oxide layer, whereas Na^+ ions remain on the surface.

Table 1: Auger electron spectroscopy relative ratios after each oxidation step.

Sample	O/Fe	C/Fe	Cl/Na	C/O
A) clean Fe surface	0.07	0.36	-	5.46
B) dried 10mM NaCl droplet	1.91	2.39	2.90	1.25
C) after H_2O/O_2 adsorption	3.04	3.12	2.42	1.02
D) after NAP O_2 adsorption	7.33	5.79	1.71	0.79

3.5 Mechanism for the formation of surface adsorbed carbonate

Based on the observations that obtained in the NAP-XPS and PM-IRRAS experiments we suggest a basic mechanism for the formation of CO_3 on the surface by the oxidation of hydrocarbons. Overall a correlation is observed from the oxidation of surface hydrocarbons and the increase in surface carbonates, in the presence of the two key reactants in corrosion, H_2O and O_2, as shown in equation 7. These are consistent with our previous observations of the formation of carbonate films in 10 mM NaCl(aq) at the air/electrolyte/iron interface.[18, 23]

$$\text{Overall surface reaction: } Fe(OH)_2 + C_xH_y + \frac{y+5}{2}O_2 + 2H_2O \rightarrow FeCO_3 + (y+6)OH \quad (7)$$
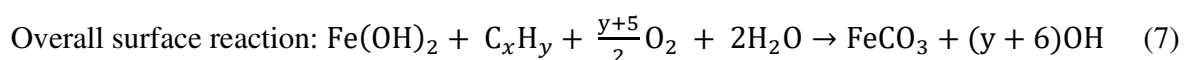
The addition of O_2 in the presence of the Cl^- and Na^+ appear to promote oxidation of the adventitious carbon, compared to the iron surface spot with no NaCl, where carbonate formation does not occur (shown in Figure 2 and Figure 4). Surface hydrocarbon impurities (C_xH_y) are known to undergo catalytic oxidation on other metal surfaces promoted with alkali metals[27], such as in the water-gas shift reaction[34], but require higher temperatures.[35] These reactions typically occur at temperatures above 350 ºC, but other studies show a relationship that the larger number of carbon chains, the lower the temperature of oxidation to CO_2.[35, 36] Based on this knowledge, some of these elementary steps may explain how the observed surface hydrocarbons are converted to carbonates. In our case, the Cl^- ions most likely pit through the oxide layer while in the liquid droplet, exposing metallic Fe sites from surface corrosion.[18] [37] Additionally, during exposure to near ambient pressures of water vapor, the NaCl may act to trap the water at the surface through hydration providing OH sites for further reaction. Once O_2 is exposed to the surface, this may allow for facile oxidation of the adventitious hydrocarbons to CO and CO_2.[38] It is also known

that metal surfaces, promoted with alkali ions, are known to easily convert to surface adsorbed surface adsorbed CO_2 to CO_3 in the presence of gas phase oxygen.[39] Other studies report hydrocarbon oxidation through a Mars Van Krevelen mechanism, where lattice oxygen atoms oxidize hydrocarbons and are replenished through exposure to additional gas phase oxygen, enabling the formation of CO_2 from CO.[40] [41] This may explain how the surface carbonate species are obtained.

On the iron surface, the presence of the ions appears to promote CO_3 formation. In surface corrosion, the Cl^- are known to pit the surface creating nucleation sites and resulting in the release of Fe^{2+} cation at the liquid/solid interface. [19] [32] [42]   In our observations in Figure 5, the decrease of the Cl 2p signals suggest the Cl^- ions migrate away from the analysis region through the native oxide layer, leaving Na^+ at the interface region. This subsurface migration of the Cl^- ions may be facilitated by the trapping of water, making more Fe^{2+} sites available for the oxidation of CO and other hydrocarbons (C_xH_y) facile after exposure to O_2. We do not observe an increase in Fe^{2+} peak area from the NAP-XPS signals, however an increase in CO and C=O species are observed during the NAP-XPS experiment (see Figure S9 in the SI), may suggest the presence of intermediate C-O or C=O species, prior to producing CO_3. A summary of the proposed mechanism, based on our observations, is shown in Figure 8 below.
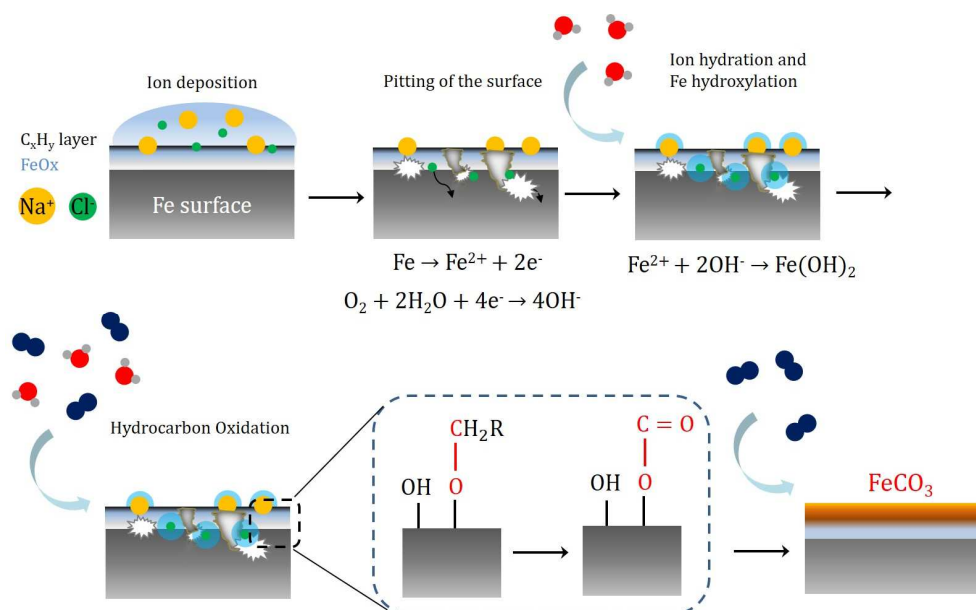

Figure 8: The schematic illustration of surface corrosion and oxidation to carbonate: (1) Cl^- ions initiate corrosion by pitting the surface when in solution, (2) exposure to water leads to ion and surface hydration, (3) oxidation of surface hydrocarbons through the formation of surface adsorbed CO and CO_2 upon the exposure of O_2 to produce iron carbonate.

The observed rates for each reactant, H_2O and O_2 in the PM-IRRAS and AES experiments show that the effect of water on the CO_3 growth is 1st order. The O_2 exposure appeared to only have an effect on the growth of CO_3 at the near ambient pressure regime (shown in Figure S7-S8) by itself, but the CO_3 growth is faster in the presence of water vapor. The NAP-XPS results show an interesting correlation between the decrease in surface hydrocarbons and the increase in carbonate

formation, but due to the several intermediate steps from water adsorption to CO_3 formation, the overall reaction rates make this fundamental reaction complex to determine the order of reaction. Further experiments are needed to ultimately uncover the oxidation mechanism for H_2O and O_2 on the surface carbonation and corrosion of iron, in the presence of ions.

In ambient environments, the hydrocarbon oxidation in ambient conditions could compete with atmospheric CO_2 adsorption. The defect sites as well as Fe-OH sites on the surface after corrosion provide basic sites, such as hydroxyl groups or oxygen sites, ideal for gas phase CO_2 adsorption. [43] Compared to our previous results at the liquid/solid interface, CO_2 adsorbs into the liquid layer, easily binding with the surface OH sites producing surface adsorbed carbonates.[18] However at the gas/solid interface, carbonation is much slower without an ionic medium to facilitate ion diffusion. In ambient conditions, gas phase O_2 is the stronger oxidant and present in higher concentrations, which allow for oxyhydroxides to form.[44] In the initial stages of oxidation presented here, $FeCO_3$ was observed the main product, which may have protected the surface temporarily from further oxidation. More oxygen exposure is required to convert $FeCO_3$ into FeOOH.[12, 45]

This experiment presented here advances our knowledge on the initial stages of iron surface oxidation that leads to corrosion under the influence of NaCl and the role of water and oxygen for the initiation stages. This emphasized the importance of surface contaminants for the composition of iron corrosion products and also the influence of Na^+ and Cl^- ions in the fundamental steps in surface corrosion. Both water and oxygen are needed with the added ions to convert the surface hydrocarbons to surface carbonates.

4.0 Conclusions

The initial stages of iron surface oxidation and corrosion were studied using NAP-XPS, PM-IRRAS and AES under the influence of NaCl ions and controlled exposure to $O_2(g)$ an H_2O vapor. Surface oxidation was measured using NAP-XPS in two stages: 1) under the variable pressures of O_2 under a constant H_2O vapor pressure of 100 mTorr, and 2) under the variable O_2 pressures with H_2O vapor pressure of 0 mTorr. Results show that water vapor is required for surface oxidation of hydrocarbons to produce carbonates. The effect of O_2 by itself did not result in apparent further oxidation to more carbonates either from the irreversibility of the reaction or from the lack of water vapor. The PM-IRRAS and AES experiments were used to measure the effect of H_2O and O_2 separately, at UHV conditions. The growth of surface carbonate was found be 1st order with respect to the water vapor exposure. The O_2 was found to have an effect near ambient pressure conditions on the oxidation of surface hydrocarbons and increased growth of surface carbonate.

The following conclusions can be reached: 1) The surface deposited hydrocarbons on Fe/NaCl are oxidized and found to correlate with the growth of carbonate in the presence of water vapor with increasing O_2 exposure. Near ambient pressure conditions, surface carbonate formation is found to follow a Langmuir isotherm model with both water and O_2. 2) The growth of surface carbonates on Fe in the presence of NaCl follows 1st order kinetics with respect to water at low exposures. 3) A mechanism is suggested that ions from the NaCl droplet corrode the surface, thus exposing Fe

sites for the catalyzed oxidation. The water vapor is necessary for the reaction to occur and may provide surface hydration of the dried NaCl droplet, to allow for ion mobility of the Na^+ and Cl^- ions. The Cl^- ions were observed to decrease in intensity in the analysis region suggesting migration towards the bulk iron, thus penetrating through native oxide layer, exposing more Fe sites for the surface reaction. Further exposure from both water and O_2 was suggested to oxidize the adventitious hydrocarbons, thus producing carbonates through surface oxidation.

This fundamental study of the initial stages of oxidation and corrosion under controlled chemical environments shows how the individual reactants in corrosion, water and O_2 with adsorbed ions, promote the conversion of hydrocarbons to produce carbonate films on iron surfaces. These findings are also important for understanding other surface catalytic and redox reactions in geochemical formation, pipeline corrosion for water quality, and environmental chemical processes.

6.0 Author contributions

CdA, MT, and KAP performed the NAP-XPS corrosion experiment at beamline 9.3.2 at the ALS under the guidance from SN and EJC. CdA analyzed and interpreted the NAP-XPS and AES data, as well as wrote the majority of the manuscript under the advisement of KAP. MT performed the PM-IRRAS and AES experiments. KAP analyzed the PM-IRRAS data, conceptualized the original research idea, and designed the experiments and wrote sections of the manuscript. All authors declare no competing interests and have given approval of the manuscript.

7.0 References

[1] M.A.J. Mazumder, Global Impact of Corrosion: Occurrence, Cost and Mitigation., Glob J Eng Sci. 5(4) (2020).

[2] K. Baranidharan, S.T. Kumaran, M. Uthayakumar, P. Parameswaran, COMPREHENSIVE REVIEW OF VARIOUS CORROSION BEHAVIOURS ON 316 STAINLESS STEEL, Metallurgical & Materials Engineering 27(2) (2021) 115-135.

[3] K.J. Pieper, R. Martin, M. Tang, L. Walters, J. Parks, S. Roy, C. Devine, M.A. Edwards, Evaluating Water Lead Levels During the Flint Water Crisis, Environmental Science & Technology 52(15) (2018) 8124-8132.

[4] C.H. Boufides, L. Gable, P.D. Jacobson, Learning from the Flint Water Crisis: Restoring and Improving Public Health Practice, Accountability, and Trust, Journal of Law Medicine & Ethics 47 (2019) 23-26.

[5] B. Kendall, A.D. Anbar, A. Kappler, K.O. Konhauser, The Global Iron Cycle, in: A.H. Knoll, D.E. Canfield, K.O. Konhauser (Eds.), Fundamentals of Geobiology John Wiley and Sons2012, pp. 65-92.

[6] W. Nie, A.J. Ding, T. Wang, V.M. Kerminen, C. George, L.K. Xue, W.X. Wang, Q.Z. Zhang, T. Petaja, X.M. Qi, X.M. Gao, X.F. Wang, X.Q. Yang, C.B. Fu, M. Kulmala, Polluted dust promotes new particle formation and growth, Scientific Reports 4 (2014).

[7] S. Zhang, D.J. DePaolo, Rates of CO2 Mineralization in Geological Carbon Storage, Accounts of Chemical Research 50(9) (2017) 2075-2084.

[8] I.S. Cole, D. Marney, The science of pipe corrosion: A review of the literature on the corrosion of ferrous metals in soils, Corrosion Science 56 (2012) 5-16.

[9] F. He, L. Gong, D.M. Fan, P.G.G. Tratnyek, G.V.V. Lowry, Quantifying the efficiency and selectivity of organohalide dechlorination by zerovalent iron, Environmental Science-Processes & Impacts 22(3) (2020) 528-542.

[10] J.Z. Huang, A. Jones, T.D. Waite, Y.L. Chen, X.P. Huang, K.M. Rosso, A. Kappler, M. Mansor, P.G. Tratnyek, H.C. Zhang, Fe(II) Redox Chemistry in the Environment, Chemical Reviews 121(13) (2021) 8161-8233.

[11] J.R. Scully, Corrosion chemistry closing comments: opportunities in corrosion science facilitated by operando experimental characterization combined with multi-scale computational modelling, Faraday Discussions 180 (2015) 577-593.

[12] R. Rodrigues, S. Gaboreau, J. Gance, I. Ignatiadis, S. Betelu, Reinforced concrete structures: A review of corrosion mechanisms and advances in electrical methods for corrosion monitoring, Construction and Building Materials 269 (2021).

[13] D.B. Patil, A.R. Sharma, Study on the Corrosion Kinetics of Iron in Acid and Base Medium, E-Journal of Chemistry 8 (2011) S358-S362.

[14] E. McCafferty, Introduction to Corrosion Science, Springer, New York, 2010.

[15] M. Veneranda, J. Aramendia, L. Bellot-Gurlet, P. Colomban, K. Castro, J.M. Madariaga, FTIR spectroscopic semi-quantification of iron phases: A new method to evaluate the protection ability index (PAI) of archaeological artefacts corrosion systems, Corrosion Science 133 (2018) 68-77.

[16] D. Persson, D. Thierry, N. LeBozec, T. Prosek, In situ infrared reflection spectroscopy studies of the initial atmospheric corrosion of Zn-Al-Mg coated steel, Corrosion Science 72 (2013) 54-63.

[17] J. Nawrocki, J. Swietlik, Analysis of Corrosion Phenomena in Water-pipe Networks, Ochrona Srodowiska 33(4) (2011) 27-40.

23

[18] C. de Alwis, M. Trought, J. Lundeen, K.A. Perrine, Effect of Cations on the Oxidation and Atmospheric Corrosion of Iron Interfaces to Minerals, Journal of Physical Chemistry A 125(36) (2021) 8047-8063.

[19] J.R. Scully, Future Frontiers in Corrosion Science and Engineering, Part II: Managing the Many Stages of Corrosion, Corrosion 75(2) (2019) 123-125.

[20] K. Lutton, W.H. Blades, J.R. Scully, P. Reinke, Influence of Chloride on Nanoscale Electrochemical Passivation Processes, Journal of Physical Chemistry C 124(17) (2020) 9289-9304.

[21] G. Chen, T. Wenga, W. Ma, F. Lin, Theoretical and experimental study of gas-phase corrosion attack of Fe under simulated municipal solid waste combustion: Influence of KCl, SO2, HCl, and H2O vapour, Applied Energy 247 (2019) 630-642.

[22] A.J.B. Muwanguzi, A.V. Karasev, J.K. Byaruhanga, P.G. Jönsson, Characterization of Chemical Composition and Microstructure of Natural Iron Ore from Muko Deposits, ISRN Materials Science 2012 (2012) 1-9.

[23] C. de Alwis, K.A. Perrine, In Situ PM-IRRAS at the Air/Electrolyte/Solid Interface Reveals Oxidation of Iron to Distinct Minerals, Journal of Physical Chemistry A 124(33) (2020) 6735-6744.

[24] E.Y.M. Mendoza, A.S. Santos, E.V. Lopez, V. Drozd, A. Durygin, J.H. Chen, S.K. Saxena, Iron oxides as efficient sorbents for CO2 capture, Journal of Materials Research and Technology-Jmr&T 8(3) (2019) 2944-2956.

[25] S. Fonna, M.I.I. Bin, Gunawarman, S. Huzni, M. Ikhsan, S. Thalib, Investigation of corrosion products formed on the surface of carbon steel exposed in Banda Aceh's atmosphere, Heliyon 7(4) (2021) e06608.

[26] G.D. Degaga, M. Trought, S. Nemsak, E.J. Crumlin, M. Seel, R. Pandey, K.A. Perrine, Investigation of N-2 adsorption on Fe3O4(001) using ambient pressure X-ray photoelectron spectroscopy and density functional theory, Journal of Chemical Physics 152(5) (2020).

[27] G.S. Parkinson, Iron oxide surfaces, Surface Science Reports 71(1) (2016) 272-365.

[28] J.J. Yeh, I. Lindau, ATOMIC SUBSHELL PHOTOIONIZATION CROSS-SECTIONS AND ASYMMETRY PARAMETERS - 1 LESS-THAN-OR-EQUAL-TO Z LESS-THAN-OR-EQUAL-TO 103, Atomic Data and Nuclear Data Tables 32(1) (1985) 1-155.

[29] E.M.G. B. L. HENKE, and J. C. DAVIS, X RAY INTERACTIONS: PHOTOABSORPTION, SCATTERING, TRANSMISSION, AND REFLECTION AT E = 50-30,000 eV, Z = 1-92, ATOMIC DATA AND NUCLEAR DATA TABLES 54(2) (1993) 181-342.

[30] A.N. Mansour, R.A. Brizzolara, Characterization of the Surface of α-FeOOH Powder by XPS, Surface Science Spectra 4(4) (1996) 357-362.

[31] G.S. Frankel, T.S. Li, J.R. Scully, Localized Corrosion: Passive Film Breakdown vs Pit Growth Stability, Journal of the Electrochemical Society 164(4) (2017) C180-C181.

[32] J. Soltis, Passivity breakdown, pit initiation and propagation of pits in metallic materials - Review, Corrosion Science 90 (2015) 5-22.

[33] Z. Liu, Y. Song, A. Rajappan, E.N. Wang, D.J. Preston, Temporal Evolution of Surface Contamination under Ultra-high Vacuum, Langmuir 38(3) (2022) 1252-1258.

[34] P. Lazar, M. Otyepka, Dissociation of Water at Iron Surfaces: Generalized Gradient Functional and Range-Separated Hybrid Functional Study, The Journal of Physical Chemistry C 116(48) (2012) 25470-25477.

[35] L. Ma, D.L. Trimm, C. Jiang, The design and testing of an autothermal reactor for the conversion of light hydrocarbons to hydrogen .1. The kinetics of the catalytic oxidation of light hydrocarbons, Applied Catalysis a-General 138(2) (1996) 275-283.

[36] Y.F.Y. Yao, OXIDATION OF ALKANES OVER NOBLE-METAL CATALYSTS, Industrial & Engineering Chemistry Product Research and Development 19(3) (1980) 293-298.

[37] V. Soulie, F. Lequien, F. Ferreira-Gomes, G. Moine, D. Feron, P. Prene, H. Moehwald, T. Zemb, H. Riegler, Salt-induced iron corrosion under evaporating sessile droplets of aqueous sodium chloride solutions, Materials and Corrosion-Werkstoffe Und Korrosion 68(9) (2017) 927-934.

[38] T.A.Semelsberger, FUELS – HYDROGEN STORAGE | Chemical Carriers, Chemistry, Molecular Sciences and Chemical Engineering, Elsevier B.V.2009, pp. 504-518.

[39] H.J. Freund, M.W. Roberts, Surface chemistry of carbon dioxide, Surface Science Reports 25(8) (1996) 225-273.

[40] Z. Ren, Z.L. Wu, W.Q. Song, W. Xiao, Y.B. Guo, J. Ding, S.L. Suib, P.X. Gao, Low temperature propane oxidation over Co3O4 based nano-array catalysts: Ni dopant effect, reaction mechanism and structural stability, Applied Catalysis B-Environmental 180 (2016) 150-160.

[41] B. Liu, W.P. Li, W.Y. Song, J. Liu, Carbonate-mediated Mars-van Krevelen mechanism for CO oxidation on cobalt-doped ceria catalysts: facet-dependence and coordination-dependence, Physical Chemistry Chemical Physics 20(23) (2018) 16045-16059.

[42] T.S. Li, J.R. Scully, G.S. Frankel, Localized Corrosion: Passive Film Breakdown vs Pit Growth Stability: Part II. A Model for Critical Pitting Temperature, Journal of the Electrochemical Society 165(9) (2018) C484-C491.

[43] E.S. Sanz-Perez, C.R. Murdock, S.A. Didas, C.W. Jones, Direct Capture of CO2 from Ambient Air, Chemical Reviews 116(19) (2016) 11840-11876.

[44] G.M. Atenas, E. Mielczarski, J.A. Mielczarski, Composition and structure of iron oxidation surface layers produced in weak acidic solutions, Journal of Colloid and Interface Science 289(1) (2005) 157-170.

[45] B.B. Xing, N. Graham, W.Z. Yu, Transformation of siderite to goethite by humic acid in the natural environment, Communications Chemistry 3(1) (2020).